Study of Liquid Weeping at a Tapered Orifice in a Bubble Column Reactor by a Computer-Aided Image Analysis Algorithm

ARTICLE *in* INDUSTRIAL & ENGINEERING CHEMISTRY RESEARCH · MARCH 2010

Impact Factor: 2.59 · DOI: 10.1021/ie901516f

5 AUTHORS, INCLUDING:

Raymond Lau
Nanyang Technological University
66 PUBLICATIONS **781** CITATIONS

Study of Liquid Weeping at a Tapered Orifice in a Bubble Column Reactor by a Computer-Aided Image Analysis Algorithm

Md. Iqbal Hossain, Si Qi Pang, Qing Xi Pang, Yanhui Yang, and Raymond Lau*

School of Chemical and Biomedical Engineering, Nanyang Technological University, 62 Nanyang Drive, Singapore 637459

Understanding the phenomenon of liquid weeping requires knowledge of the bubbling and weeping cycle. Hence, an image analysis algorithm is developed and subsequently coupled with high-speed imaging techniques to examine the different stages in the bubbling and weeping cycle automatically. The bubbling and weeping cycle is studied under various operating conditions, using the developed algorithm, coupled with high-speed imaging techniques and the pressure fluctuation measurement. The effect of orifice angle (where the orifice angle is a measure of the orifice taperness) on the liquid weeping rate is evaluated over a range of superficial orifice gas velocities and justified with the aid of the developed algorithm, coupled with high-speed imaging techniques. A gas distributor plate with negative angle orifices is recommended for improved operation of industrial bubble column reactors over the range of superficial orifice gas velocities considered in this study, because it substantially decreases the liquid weeping rate.

Introduction

A bubble column reactor commonly consists of a plenum, a column, and a disengagement section. Gas is introduced into the column section from the plenum through a gas distributor plate, in the form of bubbles. After detaching from the gas distributor plate, bubbles would pass through the continuous liquid phase in the column section and finally leave the reactor through the disengagement section. Bubble column reactors are widely employed in chemical, petrochemical, and biochemical industries, because of their excellent transport properties and simple mechanical design.[1–3] However, one of the common problems in the operation of bubble column reactors is the weeping of liquid at the gas distributor plate.[4–10] Upon the detachment of the bubbles from the gas distributor plate, liquid flows from the column section through the orifices of the gas distributor plate into the plenum for a short period of time. This phenomenon of liquid flowing from the column section into the plenum is called "liquid weeping". Liquid weeping is the result of the decrease in plenum pressure, which is due to the bubbling process at the gas distributor plate.[4] Liquid weeping can also be considered as an after-effect of the bubbling process.[5,6] Liquid weeping causes an accumulation of liquid in the plenum. This accumulated liquid gives an additional pressure drop in the plenum when gas passes through it. The accumulated liquid also results in an uneven introduction of gas into the column section. Liquid weeping can also increase the pressure drop across the gas distributor plate[7] and causes plugging or disturbances to the bubbling process. Therefore, liquid weeping at the gas distributor plate must be minimized for improved operation of bubble column reactors.

Minimization of liquid weeping at the gas distributor plate requires the understanding of the various phenomena in a complete bubbling and weeping cycle. High-speed imaging and pressure fluctuation measurement are techniques commonly used to examine the bubbling and weeping cycles under various operating conditions.[4–8] One of the problems with the use of a high-speed imaging technique is that the conventional manual frame-by-frame analysis of thousands of images of the bubbling and weeping process is a tedious and time-consuming task. The algorithm specifically needed to examine the image sequence of a bubbling and weeping process automatically is not available in the literature.

Traditionally, the bubbling and weeping cycle is classified into three different stages: (i) the bubbling stage, where a bubble is emerging from an orifice; (ii) the weeping stage, where liquid flows into the plenum; and (iii) the bridging stage, where a gas−liquid interface is formed at the orifice.[4,7] Depending on the plenum volume and superficial orifice gas velocity, doubling, pairing, and jetting may occur at the bubbling stage.[6] There is a sudden decrease in plenum pressure in the bubbling stage. The sudden decrease in pressure is followed by an increase in pressure in the plenum in the weeping and subsequent bridging stages. The increase in pressure in the weeping stage is comparatively faster than that which occurs at the bridging stage. However, in the literature, there is still a lack of a clear indication of the transitions between the stages in a cycle and their relationship with pressure fluctuation in the plenum.

The main factor that would affect the liquid weeping rate is the superficial orifice gas velocity. An increase in the superficial orifice gas velocity would reduce the liquid weeping rate. When the superficial orifice gas velocity is higher than the jetting velocity, the liquid weeping rate is considered to be negligible.[4–9] There are other factors that affect the liquid weeping rate, such as the plenum volume, the orifice dimensions, the number of orifices, and the orifice pitch distance. The liquid weeping rate decreases as the plenum volume increases, especially for orifices of small diameters.[4,5,7] However, the effect of plenum volume is small when the plenum volume is <2 L.[4] As the plenum volume increases, the frequency (as well as the magnitude) of the pressure fluctuation decreases, which, in turn, reduces the liquid weeping rate.[5]

Orifice dimensions such as the diameter and the length have a remarkable effect on the liquid weeping rate. Typically, at a constant superficial orifice gas velocity, the liquid weeping rate increases significantly with an increase in the orifice diameter if the orifice diameter is >2 mm. Simultaneous weeping and bubbling may even be observed for a large orifice diameter.[6] In some studies, no liquid weeping is found if the orifice diameter is <2 mm with a large plenum volume under quiescent

* Author to whom correspondence should be addressed. Tel.: +65 63168830. Fax: +65 67947553. E-mail: wmlau@ntu.edu.sg.

10.1021/ie901516f
Published on Web 03/12/2010

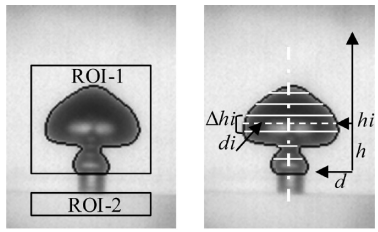

Figure 1. Image analysis: (a) bubble with a closed contour and locations of ROIs in an image frame, and (b) bubble volume determination.

water.[4,7,9,10] It is believed that, under these conditions, the surface tension force is dominant for small orifices. The liquid weeping rate is larger for an orifice with larger length but no explanation was given.[9] The effect of the number of orifices on the liquid weeping rate is more pronounced at higher superficial orifice gas velocities. The liquid weeping rate is observed to increase with the number of orifices in the gas distributor plate.[11] Speculation on the reason for this effect is that the effect of plenum volume per orifice decreases with an increase in the number of orifices. The effect of orifice pitch distance is also more significant at high superficial orifice gas velocities, and the liquid weeping rate is observed to decrease with increasing orifice pitch distance.[4] In addition to the orifice dimensions, the number of orifices, and the orifice pitch distance, the orifice taperness (which is represented by the orifice angle) also is an orifice design variable. Using a tapered orifice is a modification that can be applied to existing gas distributor plates without much complication, and it may be an effective way to reduce the liquid weeping. However, the effect of orifice angle on liquid weeping is not available in the literature.

In the present study, an image analysis algorithm is developed to eliminate the tedious and time-consuming manual analysis involved with high-speed imaging techniques in the study of the bubbling and weeping process that occurs at the gas distributor plate. The developed algorithm is coupled with high-speed imaging techniques to examine the bubbling and weeping cycle. A detail classification of the different stages in a cycle and the relationship with the pressure fluctuation in the plenum are proposed. The effect of orifice taperness (represented by the orifice angle) on the liquid weeping rate is evaluated over a range of superficial orifice gas velocity, followed by justification with the aid of the developed algorithm coupled with high-speed imaging techniques. From an industrial point of view, the effect of orifice angle is considered to be the major contribution of this present study, because it would be a criterion for the design of gas distributor plates for industrial bubble column reactors.

Image Analysis Algorithm

This algorithm consists of two functions: (i) determine the time period of a bubbling and weeping cycle, as well as the time period of each individual stage in the cycle; and (ii) compute the instantaneous orifice gas flow rate from the emerging bubble images. It is necessary to identify the objects such as bubble or liquid droplet from the respective images. Therefore, object identification and both algorithm functions are discussed in detail in the following text.

Object Identification. As shown in Figure 1, the object and background have distinct differences in contrast. The edge of an object (the object/background interface) consists of the pixels that exhibit a large change in intensity, compared with the neighboring pixels, which belong to the object itself or the background. An improved Canny edge detection method is employed to detect the edge of an object. In this method, a Gauss sigma smoothing filter is first used, to reduce noises from an image without affecting the initial gray-level values of the object edge. The image is then convolved with a two-dimensional Gauss derivative kernel, to make it smoother. The edge of an object is then detected from the smoothed image by searching for the local maxima of the modulus of the gradient vector, where the gradient vector is essentially the first intensity derivative vector of an image, along the gradient direction. A detail description of this method is given elsewhere.[12,13] The detected edge of an object may have discontinuities, because of the local blurriness on the edge or the object being out of focus. If the discontinuities on the detected edge are small, these discontinuities can be bridged using dilation with a small structural element.[14] A closed contour that closely maps the edge of the object can then be obtained, and hence, the object is considered to be identified. However, if the discontinuities are so large that dilation is unable to successfully bridge the edges, the respective object is missed and, therefore, it cannot be taken into any of the time period and instantaneous orifice gas flow rate determinations. The probability of having an out-of-focus object is low, because of the fixed locations of the emerging bubble and the falling liquid. However, large discontinuities may still occur, because of the lighting conditions and reflections from the column wall. Hence, there is a possibility of missing some objects if only the edge detection method is applied. In addition to the edge detection method, a region segmentation method is also used for the identification of the objects that cannot be identified by the edge detection method.

In the region segmentation method, an image is segmented into two regions, where one region is black and the other is white, by comparing the gray-level value of each individual pixel of the image with a preset threshold value. Between these two regions, one corresponds to the object, whereas the other corresponds to the background. The object can be easily identified assuming eight-pixel connectivity.[14] The optimum threshold value for region segmentation is determined by the Valley-Emphasis method. The gray-level value that maximizes the gray-level between-class variance (and also has a small probability of occurrence in the gray-level histogram of the image) is taken as the optimum threshold value in the Valley-Emphasis method. A detailed description of this method is given elsewhere.[15] Formulation for the optimum threshold value in the Valley-Emphasis method is given below:

$$T^* = \underset{0 \le T < L}{\mathrm{Arg\,Max}} \{(1 - p_T)(\omega_1(T)\mu_1{}^2(T) + \omega_2(T)\mu_2{}^2(T))\} \quad (1)$$

where T is a gray-level value, L the total number of distinct gray-level values in the image, and p_T the probability of the occurrence of a gray-level value T. The parameter ω_1 is the probability of all gray-level values falling in the first class (object), whereas ω_2 is the probability of all gray-level values falling in the other class (background); μ_1 and μ_2 represent the mean gray-level values of these two classes.

Time Period Determination. The entire bubbling and weeping cycle is divided into four stages: bubbling, gas−liquid interface movement, weeping, and bridging. The time period of an individual stage reflects the weight of that particular stage in the cycle; hence, the time period distribution in a cycle is essential to understand the cycle under a certain operating condition. Determining the time period of each stage, as well as that of the cycle, requires analysis of each image frame of

Table 1. Illustration of Time Period Determination

	Frame	ROI-1	ROI-2
	0	--	--
V, I	1	Connected bubble	--
V, I	2	Connected bubble	--
V, I	3	Connected bubble	--
V, I	4	Connected bubble	--
V, II	5	--	--
V, II	6	--	--
V, III	7	--	Weeping droplet/jet
V, III	8	--	Weeping droplet/jet
V, III	9	--	Weeping droplet/jet
V, IV	10	--	--
V, IV	11	--	--
	12	Connected bubble	--
	↓	Connected bubble	--

I = Bubbling stage; II = Gas-liquid interface movement stage; III = Weeping stage; IV = Bridging stage; V = Cycle.

the inputted image sequence of a bubbling and weeping cycle. Two regions of interest (ROI) are taken from an image frame in such a way that one ROI contains only the emerging bubble while the other contains only the falling liquid drop. Locations and sizes of the ROIs are defined arbitrarily by the user for each image sequence. An example image frame with the defined ROIs is shown in Figure 1a. The size of ROI-1 must be large enough to accommodate the entire bubble at the moment of its detachment. Since the primary interest of the image analysis in ROI-2 is the presence of liquid weeping, it is not necessary to include the entire liquid jet for ROI-2. The size of ROI-2 must have a width larger than the orifice diameter at the bottom of the distributor. The edge detection and the region segmentation methods described previously are both applied to each of these ROIs. For the identification of the different stages, a binary response to each ROI is determined for all the frames. For ROI-1, a positive response is given to a bubble connected to the orifice and a negative response is given otherwise. For ROI-2, a positive response is given to the presence of a weeping liquid droplet/jet and a negative response is given otherwise. The identification of the different stages can then be determined based on the binary responses on ROI-1 and ROI-2. For example, if a bubble connected to the orifice is present in ROI-1, it is considered to be in the bubbling stage. The time elapsed between the bubbling and weeping stages is considered to be in the gas−liquid interface movement stage. A sample matrix with the stored results and the criteria for the stage determination is shown in Table 1.

Instantaneous Orifice Gas Flow Rate Determination. Knowledge of the instantaneous orifice gas flow rate is very important to understanding the bubbling process at the orifice. The bubbling and weeping are two indivisible processes. Therefore, the instantaneous orifice gas flow rate during the bubbling process is also related to the subsequent weeping process. More specifically, the instantaneous orifice gas flow rate gives a measure of the decrease in pressure in the plenum that is due to the bubbling process, and this decrease in pressure actually governs the liquid weeping in a cycle. Hence, the instantaneous orifice gas flow rate also is important to understanding the weeping process. Based on the methods described in the previous section, the contour of an emerging bubble is identified from each image frame of the bubbling process, as shown in Figure 1a. Most bubbling studies consider the shape of an emerging bubble to be spherical with a cylindrical neck.[8,16,17] The bubble image in Figure 1a shows that this assumption may not give a good estimation of the actual bubble volume. Hence, with the identification of the bubble contour, the volume of the bubble is determined numerically by assuming that the bubble is symmetric about the central vertical axis. In this numerical method, the contour of the bubble is discretized into differential horizontal elements, as illustrated in Figure 1b. The volume of a differential element is considered to be the volume of the disk formed by rotating the respective horizontal element 360° along the center axis. Hence, the volume of the bubble is calculated by adding the volume of all the disks. Mathematically, the volume of the bubble is calculated as

$$v_b = \sum_{i=1}^{N} \left(\frac{\pi}{4}\right) d_i^2 \Delta h_i \tag{2}$$

where d_i and Δh_i are, respectively, the diameter and height of the disk whose center is located at the vertical location of h_i. The diameter d_i is basically the distance between the edges of the bubble image at a particular vertical location h_i. N in eq 2 is the number of differential elements/disks. The choice of N would be dependent on the degree of accuracy needed, as well as the image resolution. The parameter N used in this study is taken as the maximum vertical height of a bubble, in terms of the number of pixels. The instantaneous orifice gas flow rate during the bubbling process is then determined from the bubble volumes in two consecutive emerging bubble images, according to

$$Q_{ol_t} = \frac{v_{bl_{t+\Delta t}} - v_{bl_t}}{\Delta t} \tag{3}$$

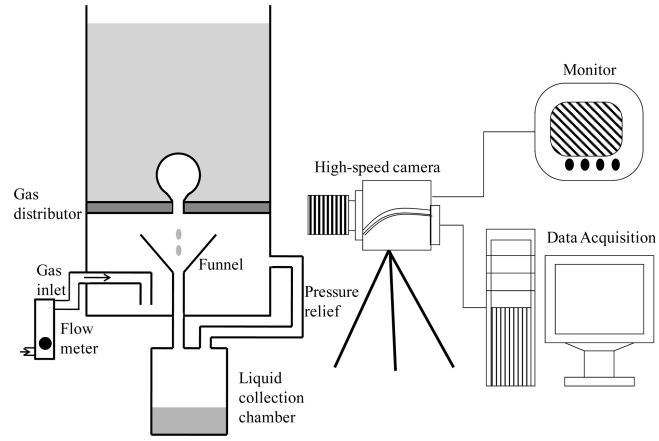

Figure 2. Experimental setup for examining the bubbling and weeping cycle, as well as for measurement of the liquid weeping.

Experimental Section

The experimental setup used in this present study is shown in Figure 2. The acrylic-made bubble column has an internal

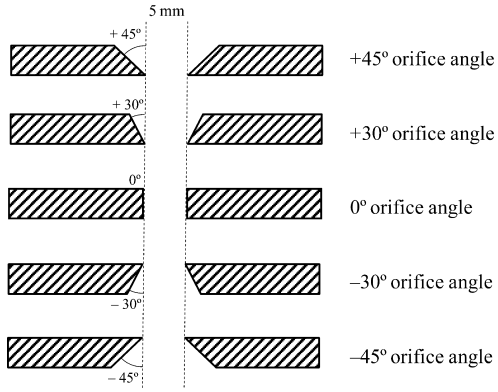

Figure 3. Five single orifice gas distributor plates with different tapered orifice angles.

diameter of 14 cm. The plenum has an average volume of 2300 cm^3 by taking into account the liquid collected at the beginning and the end of the experimental runs. The gas distributor plate has a single orifice, and the plate length is 0.5 cm. A single orifice gas distributor plate is used in this study to minimize the disturbances induced by the bubbling process at neighboring orifices. Compressed air is used as the gas source. Water is used as the liquid phase, and the static liquid height is kept at 40 cm at the beginning of each run. In the study of the bubbling and weeping cycle, an orifice angle of 0° is considered. The orifice used has a diameter of 0.5 cm. A high-speed imaging device is used to record the bubbling and weeping process at the orifice at a recording speed of 1000 Hz. A 300-W halogen light source is used to illuminate the bubble emerging and weeping process at the orifice. The curvature of the column wall is determined to have negligible image distortion when tested with square grids. The recorded image sequence of the bubbling and weeping process is examined by the developed image analysis algorithm automatically. A pressure transducer is also mounted at the plenum to measure the plenum pressure fluctuation that is due to the bubbling and weeping process at the orifice. A sampling frequency of 1000 Hz is used for the pressure transducer signals. The signal from the pressure transducer is recorded in a computer through a multichannel data acquisition system. While evaluating the effect of the orifice angle on the liquid weeping rate, five orifice angles are considered, which varied from +45° to −45°, as shown in Figure 3. The orifices used all have a smallest diameter of 0.5 cm. The superficial orifice gas velocity, which is defined as the ratio of the average volumetric gas flow rate to the minimum orifice opening area, falls within a range of 146−840 cm/s. A funnel is placed in the plenum to collect the liquid wept from the orifice. A purge stream is used to allow the wept liquid to pass through the narrow channel of the funnel. The volume of the weeping liquid is measured over a known period of time, to determine the liquid weeping rate. In the justification of the effect of orifice angle on the liquid weeping rate, only three orifice angles—such as +45°, 0°, and −45°—and a superficial orifice gas velocity of 275 cm/s, which is within the range of 146−840 cm/s, are considered. The bubbling and weeping process is recorded by a high-speed imaging device for each of these three angles in the same way as previously described. The recorded image sequences are examined by the developed image analysis algorithm automatically. The plenum pressure fluctuation due to the bubbling and weeping process is also measured by a pressure transducer for each of these three angles in the same way as that previously described.

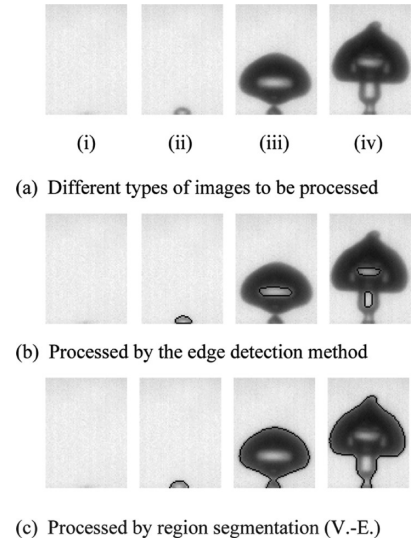

Figure 4. Evaluation of the object identification step.

Results and Discussion

Image Analysis Algorithm. Performance of the developed algorithm is evaluated and verified separately before applying it to the subsequent studies. The accuracies of object identification, time period determination, and instantaneous orifice gas flow rate determination are discussed below.

Object Identification. The object identification step is tested with (i) a single class image; (ii) an extremely unbalanced class size image; and (iii and iv) two different degrees of almost-balanced class size images shown in Figure 4a. These three image types cover the characteristics of all the images in the sequence that must be processed. Figure 4b shows that the edge detection method can treat the first and second type images (i and ii) successfully. This figure also shows that the edge detection method fails to identify some objects in the third type images (iii and iv). This failure is mainly due to the presence of a large amount of local blurriness on the edge of these objects. Figure 4c shows that the region segmentation method can treat all of the image types with reasonable accuracy. Hence, the region segmentation method is able to treat each image frame of the inputted image sequence of a bubbling and weeping process with reasonable accuracy. Since the edge detection method identifies an object by tracing the edge, it does not suffer from the problem of oversizing (or undersizing) an object and has the highest accuracy. High accuracy in sizing an object is desirable for accurate determination of the instantaneous orifice gas flow rate. Hence, the edge detection method is preferred in this algorithm, because of its high accuracy. However, since the objects with substantial local blurriness cannot be identified with the edge detection method, they cannot be taken into any of the time period and instantaneous orifice gas flow rate determinations. Failure to take any of the objects into the time period and instantaneous orifice gas flow rate determinations leads to errors in the determined time periods and instantaneous orifice gas flow rate pattern. Hence, the region segmentation method is applied to each image frame, along with the edge detection method. However, when the edge detection method fails, the contour lengths of an object obtained from these two methods are vastly different from each other. Hence, if an arbitrary difference of more than 50% between the two methods

Table 2. Comparison of the Manually and Automatically Calculated Time Periods for a Cycle, as Well as for the Individual Stages in the Cycle

operation	cycle (ms)	bubbling stage (ms)	gas−liquid interface movement stage (ms)	weeping stage (ms)	bridging stage (ms)
manual	1240	90	20	418	712
automatic	1240	90	20	416	714

Table 3. Accuracy of the Numerical Method Used to Determine the Emerging Bubble Volumes from Images

	Volume (cm^3)	
object	as determined by analytical formula[a]	as determined by numerical method[b]
sphere	$v_s = 33.5103$	$v_s = 32.9410$
cylinder	$v_c = 7.8539$	$v_c = 7.7388$

[a] $v_s = (1/6)\pi d^3$; $v_c = (\pi/4)d^2h$. [b] $(v_s,v_c) = \sum_{i=1}^{N}(\pi/4)d_i^2\Delta h_i$.

is detected, the contour obtained from the region segmentation method is used for further calculations for this object. When the contour lengths are comparable, the contour obtained from the edge detection method is used for better accuracy. Applications of both the edge detection and the region segmentation methods to each image frame tend to increase the overall computational time in this algorithm. However, with the sacrifice of a small amount of accuracy, one can use only the region segmentation method for object identification, to make the algorithm faster.

Time Period Determination. The accuracies of the time periods obtained from the developed algorithm are also tested. A comparison between the time periods determined by the developed algorithm and manual frame-by-frame analysis from a given image sequence is given in Table 2. This table shows that each of the time periods obtained from this algorithm has a good agreement with that obtained from manual frame-by-frame analysis. Hence, the developed algorithm is able to predict the time period for a cycle, as well as for each individual stage in the cycle, automatically, with reasonably high accuracy. As mentioned in the previous section, the time period of an individual stage reflects the importance of this stage in a cycle. From the time period distribution in a cycle, it is possible to identify the dominating stages in a cycle. Overall, the time period distribution in a cycle is very important to the understanding of the cycle under a certain operating condition. In addition, the time period of liquid weeping in a cycle, and then in a certain time of bubble column operation, can be taken as an indirect measure of the liquid weeping rate.

Instantaneous Orifice Gas Flow Rate Determination. The instantaneous orifice gas flow rate is determined from the bubble volumes in two consecutive emerging bubble images. Hence, the accuracy of the instantaneous orifice gas flow rate is dependent on the accuracy of the method used to determine the bubble volumes. The accuracy of the numerical method presented in eq 2 is then tested against an ideal object consisting of a sphere at the top and a cylinder at the base. The volume of the sphere, as well as that of the cylinder, are determined by both the numerical method and the analytical formula. Because the sphere and cylinder that comprise the ideal object are perfect in shape, the respective formula can give the exact volume for each of them. Hence, a comparison between the volumes determined by the numerical method and the analytical formula can prove the accuracy of the numerical method. The volume determined by the numerical method is compared with that determined by the analytical formula in Table 3 for both the sphere and the cylinder, separately. It is found that the volume determined by the numerical method is comparable with that determined by the analytical formula. Hence, the numerical method is able to determine the bubble volumes with reasonable accuracy. An experimental approach is also employed for further validation of the numerical method used. For single bubble formation, the volume of a single bubble can be approximated by dividing the volumetric gas flow rate into the plenum by the bubbling frequency. At a volumetric gas flow rate of 54 cm^3/s, the average bubble volume is determined to be 12.96 cm^3, while the numerical method gives an average bubble volume of 13.05 cm^3 and a standard deviation of 0.19 cm^3. This again demonstrates that the numerical method used to determine bubble volume in the developed image analysis algorithm would be able to compute the bubble volume with reasonable accuracy. As a result, the instantaneous orifice gas flow rate will also have reasonable accuracy. The instantaneous orifice gas flow rate is related to both the bubbling and weeping processes. Hence, the instantaneous orifice gas flow rate determined in this way can be used to explain the bubbling and weeping cycle.

Information such as the time period distribution in a cycle and the instantaneous orifice gas flow rates, which are important to the understanding of the bubbling and weeping cycle, can be determined automatically using the image analysis algorithm developed to analyze an image sequence. Hence, the developed algorithm can be coupled with high-speed imaging techniques to examine the bubbling and weeping cycle automatically.

Bubbling and Weeping Cycle. Since there is no clear indication of the transitions between the stages and their relationship with pressure fluctuation in the plenum, a more-detailed classification of the different stages in a bubbling and weeping cycle and their relationship with pressure fluctuation signal is proposed.

Detail Classification of the Stages. An illustration and detailed classification of the different stages in a cycle are shown in Figure 5. The formation of a new bubble at the orifice is considered to start at 0 ms. As shown in Figure 5b, after a bubble is detached from the orifice, there is a period of time when the gas−liquid interface is moving from the top of the orifice to the bottom of the orifice (91−110 ms). If the increase in pressure in the plenum is fast enough, the time period of gas−liquid interface movement would be sufficient for the required increase in pressure in the plenum to prevent the weeping of liquid into the plenum. As a result, no liquid weeping would be observed. Therefore, this stage of gas−liquid interface movement should be included in the analysis of liquid weeping. This stage of gas−liquid interface movement is believed to be the key controlling step for the elimination of liquid weeping. Figure 5d shows that, during the bridging stage, after liquid weeping is ceased, an oscillation of the gas−liquid interface at the bottom of the orifice can be observed. This oscillation of the gas−liquid interface would correspond to a respective oscillation in the pressure fluctuation signal in the plenum.

Relationship with Pressure Fluctuation Signal. The pressure fluctuation signal corresponding to the same bubbling and weeping cycle illustrated in Figure 5 is shown in Figure 6. It is known that the plenum pressure would decrease during the bubbling stage, because of the expansion of the emerging bubble at the orifice. However, a comparison of the pressure fluctuation signal with the high-speed image sequence indicates that the time period of the decrease in plenum pressure is always shorter than the time period of the bubbling stage obtained from the high-speed image sequence, even though the time period of the cycle is the same for both measurements. The difference in bubbling time period between the two measurements increases

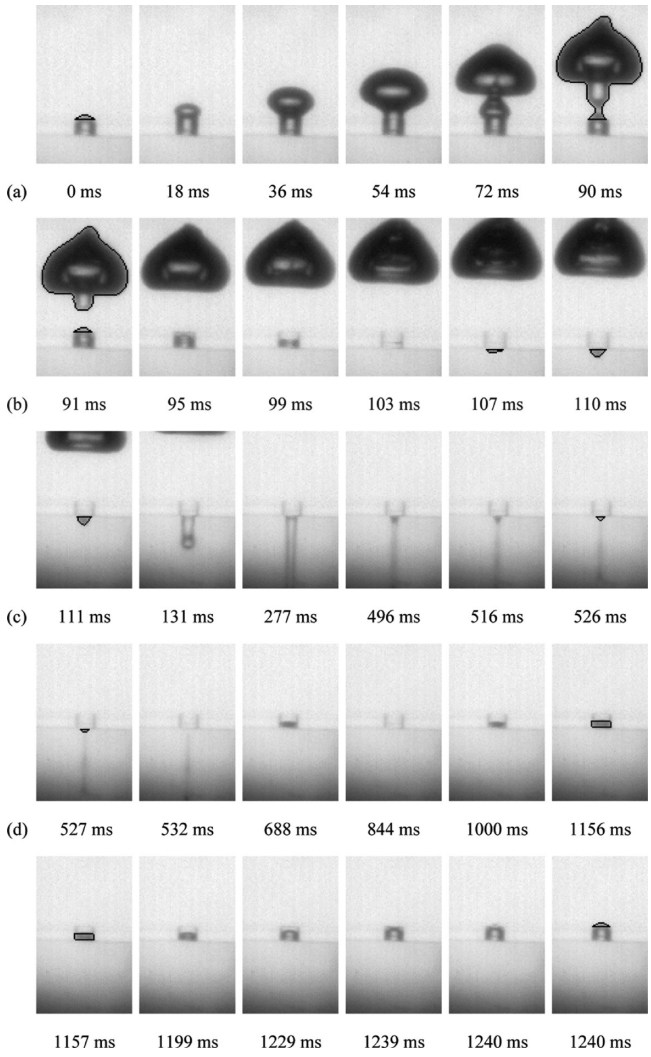

Figure 5. Illustration of a bubbling and weeping cycle: (a) bubbling stage, (b) gas−liquid interface movement stage, (c) weeping stage, and (d) bridging stage.

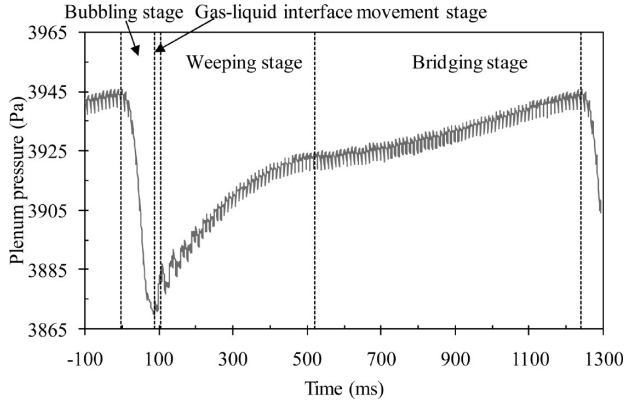

Figure 6. Plenum pressure fluctuation during a bubbling and weeping cycle.

with an increase in the flow rate of gas into the plenum. This indicates that either the plenum pressure does not start to decrease immediately after the bubble emerges from the orifice or the plenum pressure starts to increase before the bubble is detached from the orifice. Therefore, analysis is performed on the instantaneous orifice gas flow rate (Q_{olt}), using the developed image analysis algorithm to identify the correct relationship with the pressure fluctuation signal. It is assumed that the flow rate

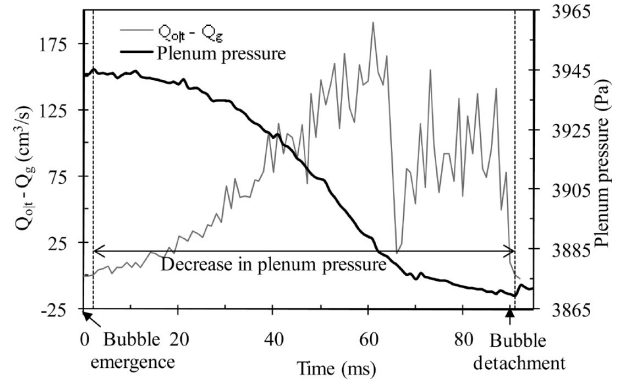

Figure 7. Comparison of the quantity ($Q_{olt} - Q_g$) and plenum pressure at the bubbling stage.

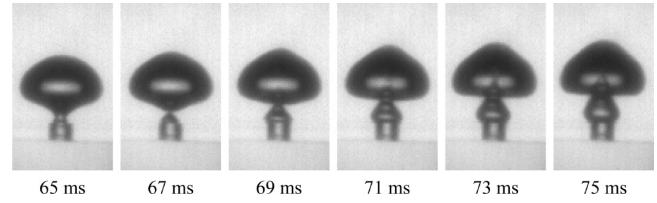

Figure 8. Illustration of the doubling formation at the bubbling stage.

of gas into the plenum, Q_g would remain constant throughout the bubbling and weeping process. The difference between Q_{olt} and Q_g can then be related to the fluctuation of plenum pressure. For example, if Q_g is less than Q_{olt}, it indicates that the gas flow rate into the plenum is smaller than the growth rate of the emerging bubble. The plenum pressure would decrease to compensate for the expansion of gas as bubble growth. A comparison of ($Q_{olt} - Q_g$) and plenum pressure versus time is shown in Figure 7. A negative value of ($Q_{olt} - Q_g$) at the beginning of the bubbling stage indicates that the bubble growth rate is smaller than the gas flow rate into the plenum. Hence, plenum pressure continues to increase, even at the beginning of the bubbling stage. The beginning of the bubbling stage should be included within the stage of increase in plenum pressure. Therefore, the maximum plenum pressure does not correspond to the beginning of the bubbling stage. The initial negative region of ($Q_{olt} - Q_g$) would be the time needed to reach maximum plenum pressure. It is observed that the length of this initial negative region increases with an increase in the flow rate of gas into the plenum. Hence, this initial region possibly causes the difference in bubbling time between the two measurements. As the rate of bubble growth exceeds the gas flow rate into the plenum, ($Q_{olt} - Q_g$) increases. The sharp decrease in ($Q_{olt} - Q_g$) is caused by the detachment of the primary bubble. However, because of the large orifice diameter, doubling is observed. As shown in Figure 8, immediately after the primary bubble detaches from the orifice, a secondary bubble is formed at the orifice. The secondary bubble would accelerate and coalescence with the primary bubble and cause an increase in ($Q_{olt} - Q_g$). Figure 7 shows that the positive region of ($Q_{olt} - Q_g$) corresponds well with the plenum pressure fluctuation results. Thus, the high-speed image sequence can be correlated with the plenum pressure fluctuation results. A comparison of the plenum pressure and ($Q_{olt} - Q_g$) shows that the formation of secondary bubbles causes a less-graduated decrease in plenum pressure. Moreover, it is found that there is a slight delay with the increase in the plenum pressure and the bubble detachment observed from the high-speed image sequence. This is possibly because the upward momentum of gas through the orifice would cause a continuous expansion of the interface after bubble

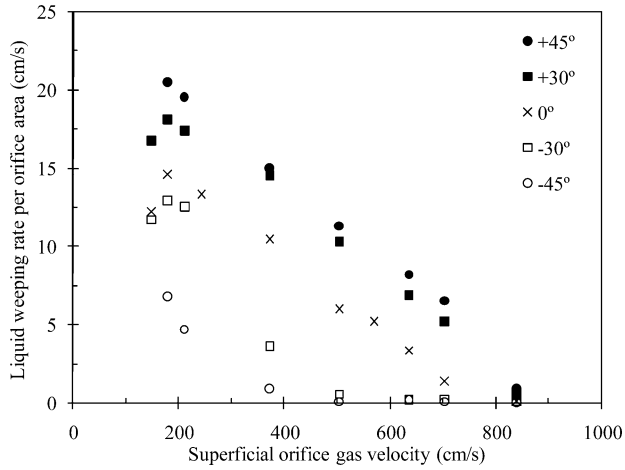

Figure 9. Effect of orifice angle on the liquid weeping rate over a range of superficial orifice gas velocities of 146−840 cm/s.

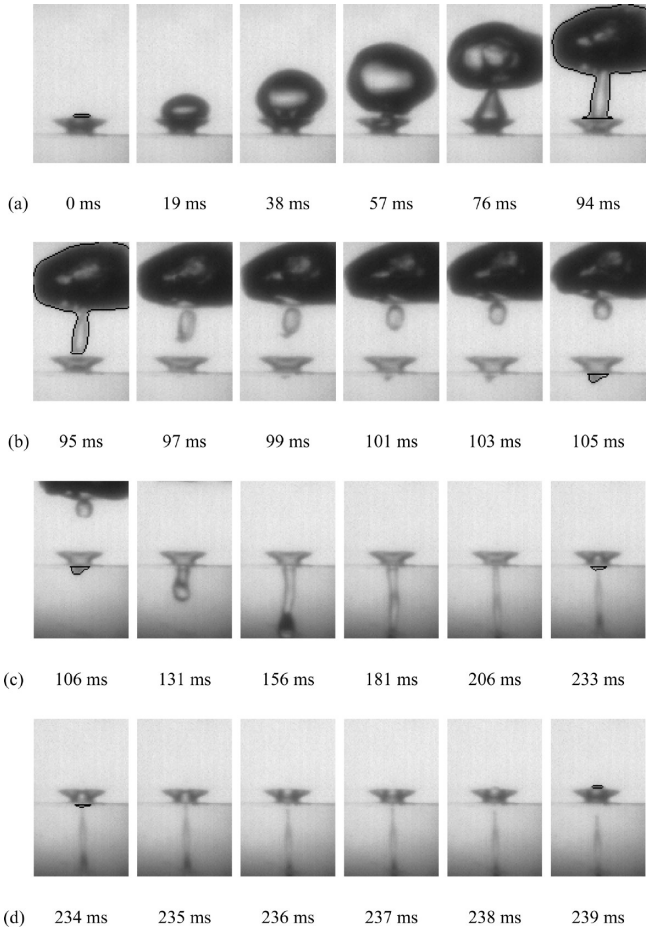

Figure 10. Illustration of the bubbling and liquid weeping cycle at a superficial orifice gas velocity of 275 cm/s for a +45° orifice: (a) bubbling stage, (b) gas−liquid interface movement stage, (c) weeping stage, and (d) bridging stage.

detachment. The interface would eventually shrink (a fraction of gas may detach from the orifice at the time of interface shrinkage) and move to the bottom of the orifice due to the low pressure in the plenum. Thus, the interface shrinkage and movement to the bottom of the orifice causes an increase in plenum pressure. Therefore, basically, the interface expansion results in the delay with increasing plenum pressure and bubble detachment. Note that interface expansion, shrinkage, and movement to the bottom of the orifice after bubble detachment

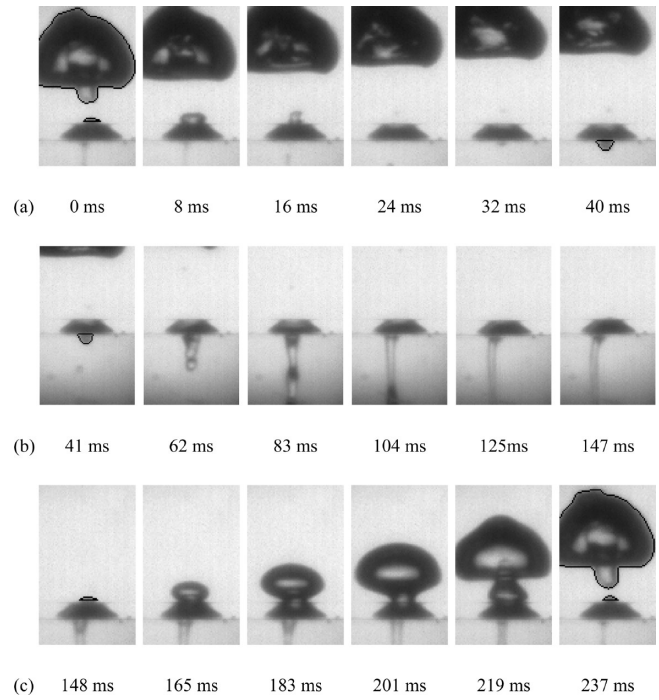

Figure 11. Illustration of the bubbling and liquid weeping cycle at a superficial orifice gas velocity of 275 cm/s for a −45° orifice: (a) gas−liquid interface movement stage, (b) weeping stage, and (c) simultaneous bubbling and weeping stage.

are taken as a single stage and termed as gas−liquid interface movement only for simplicity. However, the time period for interface expansion, as well as for the interface shrinkage in the gas−liquid interface movement stage, is observed to be very sensitive to the flow rate of gas into the plenum.

Effect of Orifice Angle. The liquid weeping rate is a measure of the volume of liquid flowing into the plenum per unit orifice area per unit time of bubble column operation. The orifice area is defined as the minimum opening area when an orifice angle other than 0° is involved. It is expressed as the average velocity of the liquid flowing through the orifice into the plenum. Liquid weeping rates for a superficial orifice gas velocity in the range of 146−840 cm/s are shown in Figure 9 for five tapered orifices with different orifice angles. This figure shows that, although the smallest openings of the orifices are all 0.5 cm in diameter, the orifice angle has a strong influence on the liquid weeping rate. A positive angle orifice gives a higher liquid weeping rate, whileas a negative angle orifice gives a lower liquid weeping rate (relative to the standard zero angle orifice) over the entire range of superficial orifice gas velocities. The result is consistent with the literature that, beyond a certain superficial orifice gas velocity, the liquid weeping rate decreases as the superficial orifice gas velocity increases,[4−9] regardless of the orifice angle. Hence, it can be concluded that the orifice angle has no influence on the trend, showing the effect of superficial orifice gas velocity on the liquid weeping rate.

The effect of orifice angle on the liquid weeping rate is justified by further analysis with the aid of the developed image analysis algorithm, coupled with high-speed imaging techniques. The image sequence of the bubbling and weeping cycle at a superficial orifice gas velocity of 275 cm/s is shown in Figures 10 and 11, for +45° and −45° orifices, respectively. A comparison between Figures 5 and 10 indicates that both 0° and +45° orifices behave in a similar manner, such that the cycle has clear distinction among the bubbling, gas−liquid interface movement, liquid weeping, and bridging stages. On the other hand, the image sequence of a −45°

Table 4. Comparison of the Time Periods for a Cycle, as Well as for the Individual Stages in the Cycle, for +45°, 0°, and −45° Orifices at a Superficial Orifice Gas Velocity of 275 cm/s

orifice angle	cycle (ms)	bubbling stage (ms)	gas−liquid interface movement stage (ms)	weeping stage (ms)	bridging stage (ms)
+45°	239	94	11	128	6
0°	240	80	32	112	16
−45°	237	90	40	197	NA

orifice (shown in Figure 11) shows simultaneous weeping and bubbling while weeping is ceased at the moment of bubble detachment. Moreover, no bridging stage is observed, because of the simultaneous weeping and bubbling behavior. A comparison of the time periods for a complete cycle, as well as for each individual stage in the cycle for +45°, 0°, and −45° orifices at a superficial orifice gas velocity of 275 cm/s, is made in Table 4. The cycle times for all the three orifice angles are comparable to each other. These cycle times are also confirmed alternatively by the analysis of the plenum pressure fluctuation signals of the three orifice angles at the same superficial orifice gas velocity.

0° Orifice vs +45° Orifice. Table 4 shows that, although the bubbling time period of a +45° orifice is higher than that of a 0° orifice, the time period needed for the gas−liquid interface to reach the bottom of the orifice upon bubble detachment and the bridging time period are significantly smaller for a +45° orifice. As a result, the weeping time period for the +45° orifice is longer than that for the 0° orifice. For a similar cycle time between the +45° orifice and the 0° orifice, a higher weeping time would give a higher total liquid weeping rate. It is believed that the opening size at the upper surface, which is

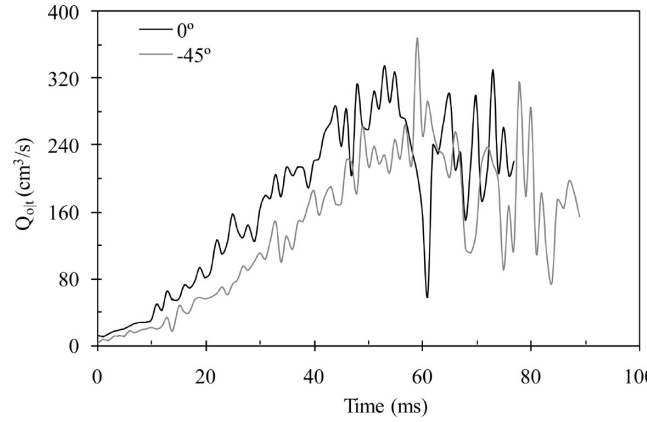

Figure 13. Comparison of the instantaneous orifice gas flow rate between the 0° and −45° orifices at a superficial orifice gas velocity of 275 cm/s.

the entrance for liquid flow from the column into the orifice, also plays an important role. At the upper surface, the +45° orifice angle gives an opening size almost three times larger than that of a 0° orifice angle. Because the opening size at the upper surface is larger, a larger amount of liquid enters into the +45° orifice from the column. As a result, a higher liquid weeping rate is obtained through the +45° orifice than through the 0° orifice. Similar behavior was observed in the case of fluid draining through the orifices connected to a tank or pipeline.[18] A round-edge orifice would yield a higher draining rate than a square-edge orifice. The square-edge orifice is equivalent to the 0° orifice, whereas the round-edge orifice is equivalent to the +45° orifice. Although the scenario of tank draining through a

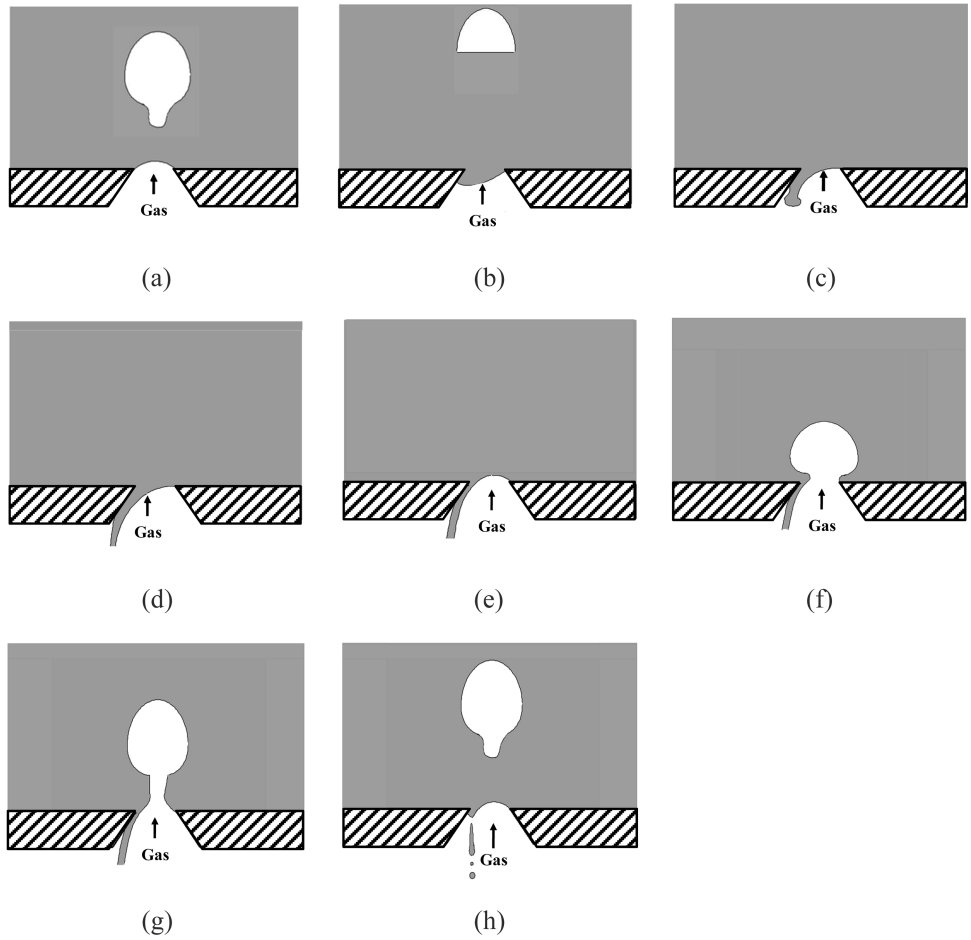

Figure 12. Illustration of the liquid weeping mechanism in a negative angle orifice.

nozzle is different from the case of liquid weeping in bubble column reactors, the behavior observed supports the difference in liquid weeping rate between the 0° and +45° orifices. The +30° orifice has a higher liquid weeping rate than that of the 0° orifice, because of the same reasons. Hence, a positive angle orifice indeed gives a higher liquid weeping rate than does the standard zero angle orifice.

0° Orifice vs −45° Orifice. The time period of each stage in a bubbling and weeping cycle for 0° and −45° orifices are also shown in Table 4. It can be realized from Table 4 that the liquid weeping time per cycle for the −45° orifice is almost double of that for the 0° orifice. Despite a longer liquid weeping time, the −45° orifice yields a lower liquid weeping rate than the 0° orifice. The reduction in liquid weeping rate at the −45° orifice is believed to be due to a different liquid weeping mechanism. An illustration that shows the key stages in the liquid weeping mechanism is shown in Figure 12. After bubble detachment, the low plenum pressure would allow the gas−liquid interface to move into the orifice region. However, the hydrodynamic instability at the negative orifice angle will cause the interface to shift toward one side of the orifice and eventually forms a weeping liquid jet (see Figures 12a−d). As the plenum pressure continues to increase, the gas bubble can emerge through the orifice without breaking the weeping liquid jet. The partial occupation of the orifice by the gas and counter-current gas−liquid flow at the orifice during the simultaneous liquid weeping and bubbling stage will thus reduce the liquid weeping rate (see Figures 12e−g). The liquid weeping ceases only until the disturbance generated during the bubble detachment breaks the weeping liquid jet and a new gas−liquid interface is re-established at the orifice (see Figure 12h). As illustrated in Figure 12, the −45° orifice angle allows the presence of gas in the orifice region at all times. The gas in the orifice is believed to be the main cause of the simultaneous liquid weeping and bubbling mechanism, which, in turn, reduces the liquid weeping rate. The instantaneous orifice gas flow rate during the entire bubbling stage is determined by the developed image analysis algorithm, and a comparison between the 0° and −45° orifices is made in Figure 13. This figure shows that the −45° orifice, indeed, has a lower instantaneous orifice gas flow rate than that of the 0° orifice, where no simultaneous weeping and bubbling is observed. Thus, a gas distributor plate with negative angle orifices is a possible modification to improve the operation of bubble column reactors.

Concluding Remarks

An automatic image analysis algorithm is developed to analyze the bubbling and weeping process using high-speed imaging techniques. The developed algorithm would increase the use of high-speed imaging techniques in the analysis of the bubbling and weeping processes. Extensive study on the bubbling and weeping cycle provides an in-depth understanding of the liquid weeping phenomenon at a single orifice gas distributor plate. Evaluation of the effect of orifice angle on the liquid weeping rate over a range of superficial orifice gas velocities shows that a negative orifice angle reduces the liquid weeping rate substantially. Hence, the orifice angle must be taken into consideration, as a criterion, in the design of gas distributor plates.

Acknowledgment

Support by AcRF Tier1 (Grant No. RG41/06) and A*STAR SERC (Grant No. 062 101 0035) is gratefully acknowledged.

Appendix

d_i = diameter of a disk formed by a rotating horizontal element
d = overall diameter
Δh_i = height of a disk formed by a rotating horizontal element
h_i = vertical location of the center of a disk
h = overall height
L = number of distinct gray-level values in an image
N = number of differential elements/disks
p_T = probability of a gray-level value T
Q_g = flow rate of gas into the plenum
Q_{olt} = instantaneous orifice gas flow rate
t = time
T = gray-level value
T^* = optimum threshold value
v_b = volume of an emerging bubble
v_c = volume of a cylinder
v_s = volume of a sphere

Greek Letters

ω = probability of a class in an image
μ = mean gray-level value of a class in an image

Literature Cited

(1) Shah, Y. T.; Kelkar, B. G.; Godbole, S. P. Design parameters estimations for bubble column reactors. *AIChE J.* **1982**, *28*, 353.
(2) Degaleesan, S.; Dudukovic, M.; Pan, Y. Experimental study of gas-induced liquid-flow structures in bubble columns. *AIChE J.* **2001**, *47*, 1913.
(3) Kantarci, N.; Borak, F.; Ulgen, K. O. Bubble column reactors. *Process. Biochem. (Oxford, U.K.)* **2005**, *40*, 2263.
(4) Akagi, Y.; Okada, K.; Kosaka, K.; Takahashi, T. Liquid weeping accompanied by bubble formation at submerged orifices. *Ind. Eng. Chem. Res.* **1987**, *26*, 1546.
(5) McCann, D. J.; Prince, R. G. H. Bubble formation and weeping at a submerged orifice. *Chem. Eng. Sci.* **1969**, *24*, 801.
(6) Miyahara, T.; Iwata, M.; Takahashi, T. Bubble formation pattern with weeping at a submerged orifice. *J. Chem. Eng. Jpn.* **1984**, *17*, 592.
(7) Peng, W. L.; Yang, G.; Fan, L. -S. Experimental studies of liquid weeping and bubbling phenomena at submerged orifices. *Ind. Eng. Chem. Res.* **2002**, *41*, 1666.
(8) Zhang, W.; Tan, R. B. H. A model for bubble formation and weeping at a submerged orifice with liquid cross-flow. *Chem. Eng. Sci.* **2003**, *58*, 287.
(9) Che, D. F.; Chen, J. J. J. Bubble formation and liquid weeping at an orifice submerged in a liquid. *Chem. Eng. Technol.* **1990**, *62*, 947.
(10) Klug, P.; Vogelpohl, A. Bubble formation with superimposed liquid motion at single-hole plates and sieve plates. *Ger. Chem. Eng.* **1983**, *6*, 311.
(11) Lockett, M. J.; Banik, S. Weeping from sieve trays. *Ind. Eng. Chem. Process Des. Dev.* **1986**, *25*, 561.
(12) Canny, J. A computational approach to edge detection. *IEEE Trans. Patt. Anal. Machin. Intell.* **1986**, *8*, 679.
(13) Wenyin, Z.; Ningde, J.; Xia, L.; Zhiqiang, N. Bubble image segmentation of gas/liquid two-phase flow based on improved canny operator. *Int. Conf. Comput. Sci. Software Eng.* **2008**, 799.
(14) Gonzalez, R. C.; Woods, R. E. *Digital Image Processing*, 2nd edition; PHIPE, Pearson Education: Upper Saddle River, NJ, 2002. (ISBN No. 0-13-094650)
(15) Ng, H.-F. Automatic thresholding for defect detection. *Pattern Recognit. Lett.* **2006**, *27*, 1644.
(16) Yang, G. Q.; Luo, X.; Lau, R.; Fan, L.-S. Bubble formation in high-pressure liquid-solid suspensions with plenum pressure fluctuation. *AIChE J.* **2000**, *46*, 2162.
(17) Xiao, Z.; Tan, R. B. H. A model for bubble−bubble and bubble−wall interaction in bubble formation. *AIChE J.* **2006**, *52*, 86.
(18) Franzini, J. B.; Finnemore, E. J. Fluid Mechanics with Engineering Applications, Ninth Edition; WCB/McGraw−Hill: New York, 1997. (ISBN No. 0-07-114214-2).

Received for review September 27, 2009
Revised manuscript received February 8, 2010
Accepted February 25, 2010

IE901516F